ELSEVIER

Chemical Geology 244 (2007) 483–492

CHEMICAL GEOLOGY
INCLUDING ISOTOPE GEOSCIENCE

www.elsevier.com/locate/chemgeo

Paleoredox, biotic and sulfur-isotopic changes associated with the end-Permian mass extinction in the western Tethys

P. Gorjan [a,*], K. Kaiho [a], T. Kakegawa [b], S. Niitsuma [b], Z.Q. Chen [c], Y. Kajiwara [d], A. Nicora [e]

[a] *Institute of Geology and Paleontology, Tohoku University, Sendai 980-8578, Japan*
[b] *Institute of Mineralogy, Petrology, and Economic Geology, Tohoku University, Sendai 980-8578, Japan*
[c] *School of Earth and Geographical Sciences, University of Western Australia, 35 Stirling Highway, Crawley, WA 6009, Australia*
[d] *Institute of Geoscience, University of Tsukuba, Ibaraki 305-8571, Japan*
[e] *Dipartimento di Scienze della Terra, via Mangiagalli 34, 20133, Milan, Italy*

Received 7 August 2006; received in revised form 30 June 2007; accepted 3 July 2007

Editor: J. Fein

Abstract

Detailed (cm-scale) %S, %TOC (total organic carbon), $\delta^{34}S_{sulfide}$, and pyrite morphological analysis of the Permian–Triassic boundary beds at the Bulla section, northern Italy, suggests that marine waters at this site saw the influx of two dysoxic–euxinic intervals that mark the end-Permian extinction event. This suggests reduced oxygen conditions, and the presence of H_2S, is the cause of the end-Permian extinction. The Bulla section also shows three troughs in $\delta^{34}S_{sulfate}$, of which the latter two coincide with the dysoxic–euxinic intervals. This suggests that the latter two $\delta^{34}S_{sulfate}$ troughs are the result of H_2S oxidation in surface waters, but the first trough is the result of a different mechanism. We propose that H_2S was oxidized in another region, either to low $\delta^{34}S_{sulfate}$ water or elemental S, which then moved to the Bulla area. At the Balvany section, Hungary, there are two $\delta^{34}S_{sulfate}$ troughs near the extinction and no evidence of euxinia. A similar mechanism to the first Bulla $\delta^{34}S_{sulfate}$ trough is proposed, with the suggestion that these waters were also depleted in oxygen in order to effect the extinction at Balvany.

Keywords: Mass extinctions; Isotopes; Sulfur; Permian; Triassic; Anoxia/euxinia

1. Introduction

The end-Permian mass extinction saw the elimination of ~90% of marine and ~70% of terrestrial species (Erwin, 1994), being the most devastating blow to life in the Phanerozoic. Yet despite the intense interest on this event a consensus on the cause has not been achieved. Suggested causes include a bolide impact (Kaiho et al., 2001; Becker et al., 2001), massive volcanic activity from the Siberian Traps (Kamo et al., 2003), reduced atmospheric oxygen content (Weidlich et al., 2003; Huey and Ward, 2005), and dissociation of methane hydrates causing a super-greenhouse effect (Retallack, 1999).

Recently, models explaining the mass extinction as a result of the spread of anoxic or euxinic waters have gained some momentum (Wignall and Twitchett, 2002;

* Corresponding author.
E-mail address: psgorjan@yahoo.com (P. Gorjan).

0009-2541/$ - see front matter © 2007 Elsevier B.V. All rights reserved.
doi:10.1016/j.chemgeo.2007.07.003

Kump et al., 2005), based on the prevalence of sections that show evidence of anoxia or euxinia around the P–Tr boundary (e.g., Wignall et al., 1998; Wignall and Twitchett, 2002; Grice et al., 2005; Riccardi et al., 2006).

Also recognized at the end-Permian (or Permian–Triassic) mass extinction is a perturbation in the sulfur cycle, as seen in the isotopic ratio of seawater sulfate ($\delta^{34}S_{sulfate}$). Kaiho et al. (2001) showed a massive decrease in $\delta^{34}S_{sulfate}$ coincident with the end-Permian mass extinction horizon at the Meishan section (China). In 2004, Newton et al. published a $\delta^{34}S_{sulfate}$ profile of the Permian–Triassic beds of Siusi, northern Italy. These data showed substantial fluctuations, although a clear decline associated with the mass extinction horizon was not well established, due to a lower sampling density. More recently, Kaiho et al. (2006a) demonstrated a $\delta^{34}S_{sulfate}$ decline at the Balvany section (Hungary). Although the $\delta^{34}S_{sulfate}$ decline is not as severe as the Meishan section (a ~10‰ decline at Balvany compared to a ~25‰ decline at Meishan), it does coincide with the mass extinction horizon. Like the actual extinction, this $\delta^{34}S_{sulfate}$ movement has been attributed to either a bolide impact (e.g., Kaiho et al., 2001) or the movement of euxinic waters (e.g., Newton et al., 2004). In a more complex mechanism, Kaiho et al. (2006b) propose an increase in the rate of sulfide oxidation relative to the rate of sulfate reduction due to degassing of H_2S from stratified intermediate-depth water rich in H_2S.

In a broader context, Riccardi et al. (2006) shows $\delta^{34}S_{sulfate}$ instability throughout the Changxingian (at the Meishan and Shangsi sections, China). However, these fluctuations are not interpreted as primary seawater $\delta^{34}S_{sulfate}$ changes.

Here we undertake an analysis of sulfide (%S), total organic carbon (TOC), sulfide-sulfur isotope ratios ($\delta^{34}S_{sulfide}$), pyrite framboid diameter, as well as paleontological analysis, in end-Permian sediments of the Bulla section in order to correlate the extinction with any changes in paleoredox conditions. We also present new $\delta^{34}S_{sulfate}$ data for the Bulla section to compare with the paleontological and paleoredox data. Furthermore, new sulfide content (%S by weight), total organic carbon (TOC), and $\delta^{34}S_{sulfide}$ data from the Balvany section were determined for comparison with the Bulla section data. We sampled at cm-scale intervals across the P–Tr boundary in order to observe biotic and geochemical changes on a timescale comparable to the extinction, which is believed to have been rapid, possibly less than 30 000 years (Rampino and Adler, 1998; Jin et al., 2000; Twitchett et al., 2001; Erwin et al., 2002; Rampino et al., 2002).

1.1. Geology and extinction horizon

The Bulla section lies between the towns of Castelrotto and Ortisei, northern Italy (Fig. 1). The lithology and stratigraphy are typical of the Italian Dolomites region. In the Late Permian (during deposition of the upper Bellerophon Formation) the region was located at an inner-shelf setting during a stage of tectonic quiescence (Massari and Neri, 1997). Throughout the Dolomites region the top 0.5–2 m of the Bellerophon Formation consists of dark marls and limestones, recording a transgression of shallow-marine conditions over previously restricted lagoonal and sabkha settings (Broglio Loriga and Cassinis, 1992). A further transgression saw the deposition of the Tesero Oolite Horizon, the basal member of the Werfen Formation (Broglio Loriga and Cassinis, 1992).

The base of bed 8 is taken as the 0 cm point in the measured section for this study (Fig. 2). The top of the Bellerophon Formation is marked by a black limestone layer. The base of the overlying Tesero Member is a bioclastic packstone–grainstone, followed by an oolitic grainstone. The P–Tr boundary, defined by the first appearance of the conodont *Hindeodus parvus* (Yin et al., 2001), occurs approximately halfway up the Tesero Member. At Bulla this is ~1.3 m above the Bellerophon–Werfen contact (in bed 12; Perri, 1991). The extinction (see below) is clearly below the P–Tr boundary.

The end-Permian extinction pattern in the Italian Dolomites has been determined at the Val Badia (Cirilli et al., 1998) and Tesero (Broglio Loriga and Cassinis, 1992; Rampino and Adler, 1998) sections at comparable sampling intervals to this study. At Val Badia the disappearance of milliolids, nodosinellids, and fusulinids (all foraminifers that were extinct by the end of the Permian) occurs within a ~30 cm interval, beginning ~10 cm below the first oolite bed of the Tesero Member.

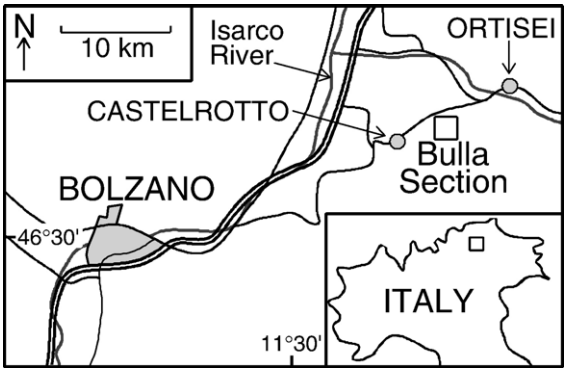

Fig. 1. Map showing location of the Bulla section, northern Italy.

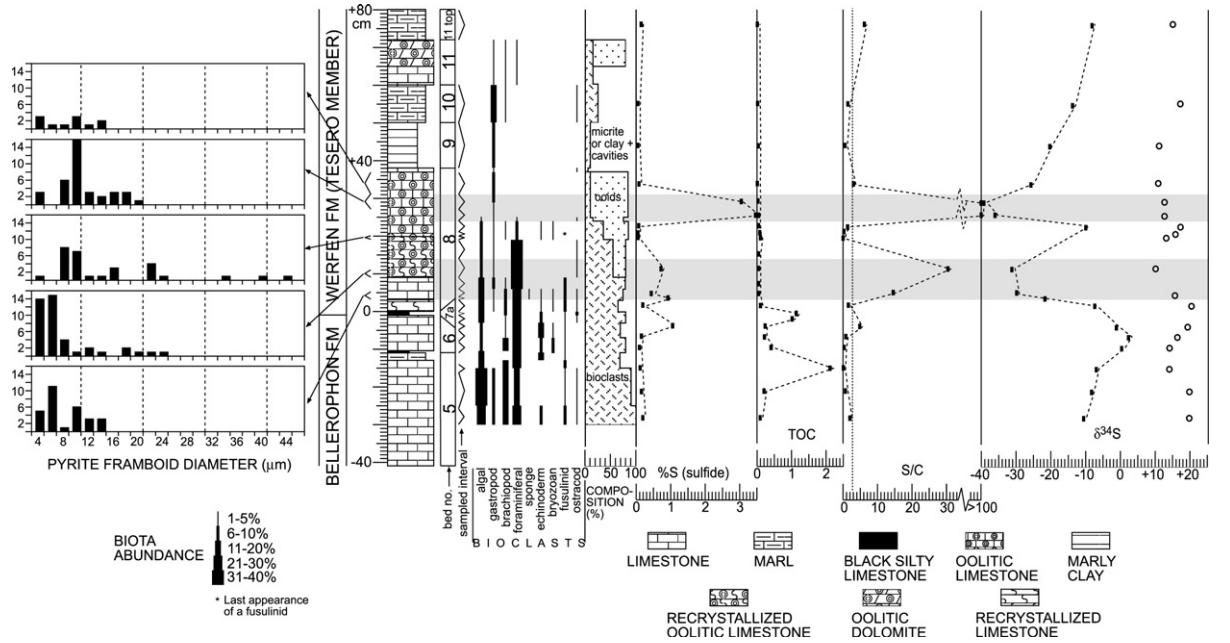

Fig. 2. Log of the Bulla section with geochemical, pyrite framboid diameter, and paleontological results plotted alongside. S/C is the ratio of %S (sulfide) and TOC, in the previous two columns. Dashed line in the S/C column is at 2.8, which is the average ratio of 'normal marine' sediments (see text). In the $\delta^{34}S$ column open circles refer to sulfate ($\delta^{34}S_{sulfate}$) and closed squares to sulfide ($\delta^{34}S_{sulfide}$). Note that 'sampled interval' on figure applies only to the geochemical data, paleontological data was determined from continuous thin sections in bed 8. Horizontal gray bands show sampled horizons with high S/C ratios.

The Hungarian Permian–Triassic Balvany section (section location map in Haas et al., 2006; and column shown in Fig. 3) is composed of the dark gray limestone and marl beds of the upper Nagyvisnyo Formation. These beds contain abundant and diverse bioclasts, suggesting a shallow, warm and oxygenated sea (Haas et al., 2006). An increase in siliclastic deposition, possibly due to terrestrial vegetation loss associated with the extinction, creates the shale of bed 12. The overlying bed 13 is a stromatolitic limestone, with no subaerial exposure, suggesting a subtidal setting. The extinction level at Balvany has been determined by the disappearance of fusulinid bioclasts (Kaiho et al., 2006b) within bed 6.

Both the Bulla and Balvany sections were located on the western side the ancient Tethys Sea (Fig. 4).

2. Methods

Detailed sampling (cm-scale) of the Bulla section was undertaken across the end-Permian extinction interval. The Balvany samples analyzed in this study are the same as the ones used in Kaiho et al. (2006b).

Sedimentary sulfide was extracted from 1 to 5 g of crushed sample. The sulfide extraction procedure is based on the method presented by Canfield et al. (1986). Sulfide was removed from the sample by reaction with an excess of acidified ~1 M $CrCl_2$ solution. The mixture was boiled until all H_2S was evolved from reaction of Cr^{2+} with sulfide. The H_2S was trapped as Ag_2S by bubbling through an $AgNO_3$ solution. The Ag_2S was collected by filtration, dried, and weighed. Stoichiometric calculations converted the Ag_2S mass to %S in the sample.

Carbonate-associated sulfate (CAS) was extracted from crushed carbonate sediments that were previously washed in 10% NaOCl solution for 24 h and then rinsed in deionized water. The carbonate was then dissolved in 4 M HCl in a nitrogen atmosphere to prevent oxidation of any H_2S formed by reaction of HCl with monosulfides. The mixture was then filtered through a 0.45 μm pore-sized membrane and $BaCl_2$ added to the filtrate to precipitate $BaSO_4$. This method is based on previous CAS isotopic studies (e.g., Newton et al., 2004).

Isotopic determinations were carried out using the EA-IRMS (elemental analyzer-isotope-ratio mass spectrometer) method on a MAT-Finnigan 252 mass spectrometer. $\delta^{34}S$ results are compared against the CDT (Canyon Diablo Troilite) standard. Errors for replicate samples are within ±0.5‰.

Total organic carbon (TOC) was determined by treating powdered samples with 6 M HCl to remove

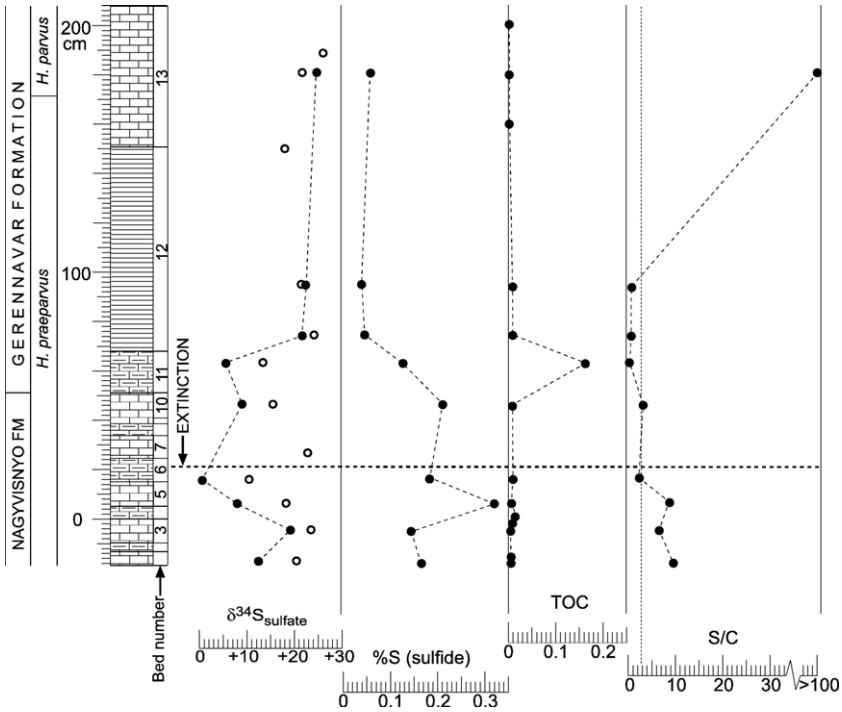

Fig. 3. New $\delta^{34}S_{sulfide}$, %S, TOC, and S/C ratio data for the Balvany section. $\delta^{34}S_{sulfate}$ (open circles), and extinction level, from Kaiho et al. (2006b). Note that the TOC and %S scales are 1/10th that of the Bulla section. Lithological legend in Fig. 2.

carbonate, followed by carbon content measurement using a Flash EA1112 elemental analyzer at Shoko Co. Ltd., Tokyo.

Thin sections were made of the Bulla section sampled intervals, and continuously for bed 8, and observed under a transmitted-light microscope to determine changes of biotic components in thin section. The quantitative point-count data of major fossil components (Fig. 2) from each thin section are based on observation of average area of 5×8 cm^2 in one sample. Then percentages of various skeletal components, micrite, ooids and cavities were combined to yield mean abundance of each composition for the sample.

Polished blocks of selected Bulla samples were also made to observe the sulfide under a reflected-light

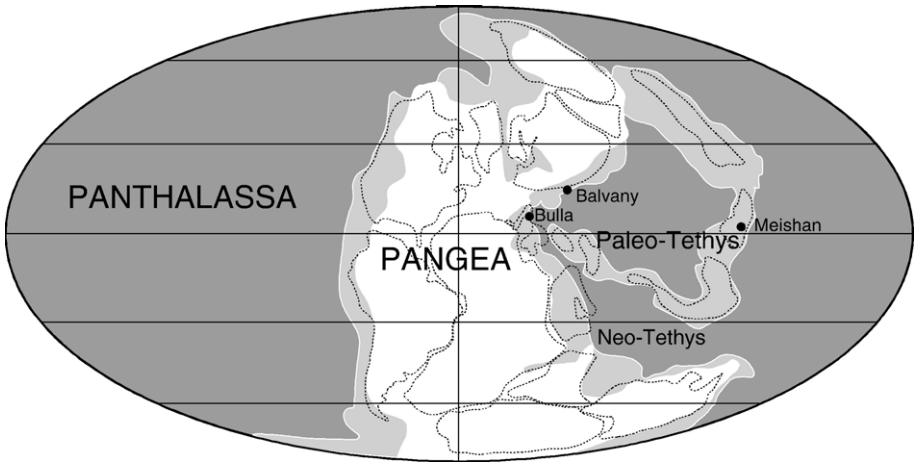

Fig. 4. Permian–Triassic paleogeographic reconstruction showing the location of the Bulla, Balvany and Meishan sections. Base map from Golonka and Ford (2000).

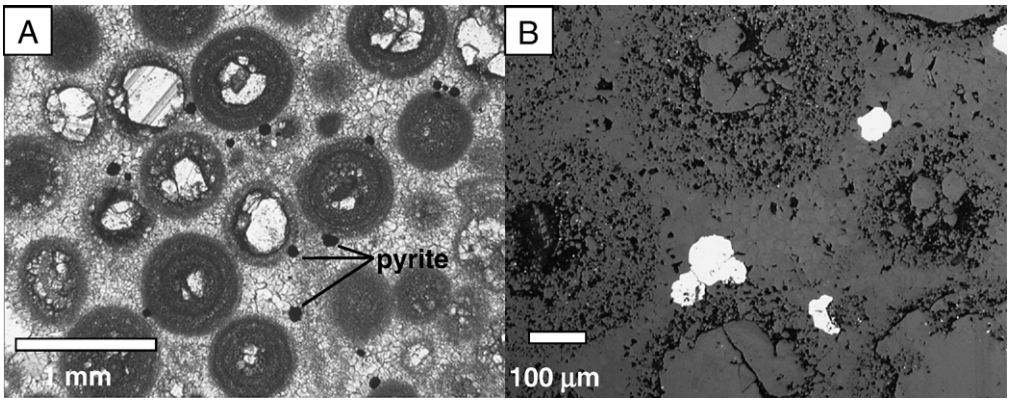

Fig. 5. Microphotographs of (A) ooids and euhedral matrix pyrite under transmitted light (from high S/C ratio horizon, 27–31 cm above bed 8 base); (B) euhedral matrix pyrite (large white blots) and framboidal pyrite (small white points within ooids), under reflected light (27–31 cm above bed 8 base). Note the absence of any veining that could lead to late-diagenetic pyrite formation.

microscope; and to measure framboid diameters using backscattered electron microscopy (JEOL JXA-8800 electron microscope).

3. Results

3.1. Bulla section samples

All results for the Bulla section are shown in Fig. 2.

Sulfide content is generally <0.25% by weight. However, between mid-bed 6 and mid-bed 8 all but one sample exceeds 0.5%; and at 24–31 cm above bed 8 base %S values are ~3%.

Total organic carbon content (TOC) fluctuates greatly below bed 8, between 0.10 and 2.15% (by weight), with all but one value above 0.2%. In bed 8 and above TOC is uniformly below 0.1%.

S/C (sulfide %/TOC) ratios vary widely, with high values (>10) at two intervals in bed 8 (actual S/C ratios are >100 for samples 24–31 cm above the base of bed 8). These high S/C ratio intervals coincide with decreased $\delta^{34}S_{sulfide}$ values. $\delta^{34}S_{sulfide}$ is normally ~−10‰ or above, but at the high S/C ratio intervals values decrease to below −30‰.

At Bulla $\delta^{34}S_{sulfate}$ fluctuates between ~+11‰ and ~+20‰. Three clear troughs can be seen, the lowest value occurring in the second trough. The latter two troughs coincide with horizons of lowered $\delta^{34}S_{sulfide}$ values and high S/C ratios (Fig. 2).

Analysis of thin sections shows that abundant and diverse allochem assemblages occur in beds 5, 6, and the lowest 9 cm of bed 8. With the beginning of oolite deposition there is a decline in bioclast content (gradually decreasing from ~80% to ~10%). Biodiversity decreases abruptly at 24–25 cm above the base of bed 8. The last continuous fusulinid occurrence is at 9 cm. There are fusulinids above this (the last fusulinid appearance is at 22 cm), but they may be reworked (Rampino and Adler, 1998). We suggest the interval 9–25 cm above the base of bed 8 is the extinction level.

Under transmitted light the major form of pyrite is euhedral (generally 50–200 µm in diameter) which occurs within the carbonate matrix (Fig. 5A). Reflected-light microscopic analysis of polished thin section shows that pyrite is the dominant sulfide (Fig. 5B). Backscattered electron microscopic imagery shows that euhedral crystals are formed around framboids (Fig. 6). Diameter measurements of those framboids are presented as histograms in Fig. 2. Minor amounts of pyrite also occur within ooids, as small framboids (generally under 5 µm diameter) (Fig. 5B).

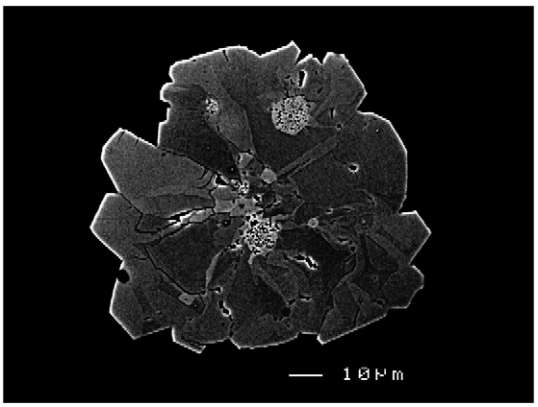

Fig. 6. Backscattered electron microscope image of a euhedral pyrite crystal. Two framboids can be seen (at center and at top) within the crystal. Note 10 micro-meter scale bar.

3.2. Balvany section samples

New $\delta^{34}S_{sulfide}$, %S, TOC, and S/C data are plotted for the Balvany section in Fig. 3, alongside previously-published $\delta^{34}S_{sulfate}$ data (from Kaiho et al., 2006b). $\delta^{34}S$ below bed 12 at Balvany is consistently 10–15‰ more negative than the $\delta^{34}S_{sulfate}$, and does not show large declines during the $\delta^{34}S_{sulfate}$ troughs (as at Bulla). In beds 12 and 13 $\delta^{34}S_{sulfide}$ is similar in value to $\delta^{34}S_{sulfate}$. %S and TOC at Balvany is about 10 times lower than at Bulla. S/C ratios are mainly around 2.8 or below. Higher S/C values in beds 1 to 5 (~10) and 13 (>100) may not be reliable indicators of euxinia as the TOC values are extremely low.

4. Discussion

4.1. Paleoredox indicators

Three sets of paleoredox indicators are available for the Bulla section in this study: S/C ratios, pyrite framboid diameter, and bioclast abundance.

Classical studies on S/C ratios (e.g., Raiswell and Berner, 1986) have shown that in 'normal marine' sediments (i.e., non-euxinic conditions, where bacterial sulfate reduction (BSR) is limited by organic matter input) the S/C ratio will average around 2.8. This occurs because BSR is limited by organic matter input to the sediment. In contrast, a euxinic environment has sulfide (H_2S) freely available in the water column to react with as much iron as can be supplied to form pyrite (FeS_2), leading to much higher S/C ratios. Most of the P–Tr succession at the Bulla section records S/C ratios typical of non-euxinic conditions (i.e., ~2.8 or below). However, there are two intervals within bed 8 showing elevated S/C ratios (Fig. 2), suggesting sedimentation in an euxinic environment.

As a separate indicator of paleoredox conditions we analyzed the pyrite framboid diameters (framboids overgrown by euhedral crystals) of five intervals of bed 8. Several studies (e.g., Wilkin and Barnes, 1996; Wilkin et al., 1996, 1997; Wignall and Newton, 1998) have demonstrated that pyrite framboids formed under euxinic conditions will be generally <6 μm and rarely above 12 μm. Framboids formed in an environment with a relatively high oxygen content show a long 'tail' in the histogram, with some framboids up to ~50 μm in diameter.

The pyrite framboid diameter data of bed 8 suggests that there were not exclusive euxinic conditions during the high S/C ratio intervals (3–14 cm and 24–31 cm). Rather, the framboidal diameter data suggests dysoxia at these levels.

Thus, the S/C and framboidal pyrite diameter data appear to give contradictory results. The former suggesting euxinia, the latter only dysoxia. In order to reconcile these data sets we propose that there was dysoxic conditions with intermittent euxinia (perhaps rapidly alternating, e.g., seasonal). We suggest that the extra sulfur was added to the sediment (precipitated onto existing framboids) during euxinic pulses, which provided ^{32}S-enriched sulfur compared to that formed by BSR within the sediment at this site (i.e., sulfur having a lower $\delta^{34}S_{sulfide}$ value). Euhedral crystals occur when excess iron and sulfide slowly crystallise within the sediment during early diagenesis (Kalliokoski and Cathles, 1969; Raiswell, 1982), when porewater sulfide concentrations are reduced so that monosulfides, a precursor for framboids, do not become supersaturated (Wang and Morse, 1995). In the Bulla case, H_2S could be added to the shallow pore spaces during euxinic pulses, and when the euxinia retreats sulfide could be diluted enough to create euhedral pyrite.

$\delta^{34}S_{sulfide}$ values drop dramatically coincident with the high S/C horizons. This is consistent with an alternative source of sulfide to that being produced within the sediment at this site. Euhedral pyrite in the low S/C intervals will develop from sulfate in porewater as BSR reduces it, fueled by the available organic matter. However, in the high S/C horizons there is insufficient organic matter to account for all the sulfide. Thus, sulfide must be introduced from outside the pores.

The low $\delta^{34}S_{sulfide}$ values are also consistent with BSR operating in the water column (and not the sediment), allowing an increase in the fractionation between sulfate and sulfide due to the open-system conditions (i.e., abundant sulfate is available for reduction) and the cycling of S between reducing and disproportionating bacteria at the chemocline (Canfield, 2001). As a parallel, sulfides of the euxinic Black Sea (both water-column H_2S and sedimentary pyrite) have $\delta^{34}S_{sulfide}$ values typically in the range −20 to −40‰ (Sweeney and Kaplan, 1980; Calvert et al., 1996; Lyons, 1997).

There is no evidence of later generation sulfide addition by hydrothermal activity, which would be associated with veining and multi-metallic sulfides, such as ZnS and PbS (Fig. 4). Thus, we rule this out as a sulfur source.

Euxinia has been demonstrated in several geographically diverse P–Tr sections: in the eastern Tethys (South China) and northern margins of the Gondwana (Western Australia) (Grice et al., 2005); the Boreal seas (Wignall et al., 1998; Nielsen and Shen, 2004); western Panthalassan margin (Ursula Creek section, British Columbia, Canada; Wignall and Newton, 2003); and

Panthalassan pelagic sediments (high S/C ratios) (Kajiwara et al., 1994). Thus, it is not surprising that it should exist at the Bulla site in the western Tethys.

It is important to note that the dysoxic–euxinic conditions determined here occur partly in oolitic sediments. As oolites are indicative of shallow, high-energy and oxic environments (Tucker and Wright, 1990, pp. 6–9), it suggests that the euxinic input must have been intense and consistent to overcome the oxidative conditions. It is therefore not surprising for extinctions to occur in such a scenario.

4.2. Sequence of paleoredox and biotic changes at Bulla

We suggest the following sequence of events in bed 8 at the Bulla section:

From 0 to 3 cm: There are oxic conditions (or no significant dysoxia), as testified to by the abundant bioclasts, no elevated S/C ratios, and high $\delta^{34}S_{sulfide}$ values.

From 3 to 5 cm: This is the beginning of the first influx of dysoxic–euxinic conditions, suggested by pyrite framboid size data (the majority of framboids are <6 μm, and no larger than 15 μm) S/C ratio (>10), and $\delta^{34}S_{sulfide}$ (<-20‰) data. In contrast, abundant and diversified bioclasts indicate oxic conditions. However, this dysoxic–euxinic interval is not as intense as at 6–10 cm and especially 24–31 cm, judging from S/C ratios. This may be reason why biota are present at this interval but not at later dysoxic–euxinic intervals.

From 5 to 9 cm: This may mark an intensifying of dysoxic–euxinic conditions as echinoderms, byrozoans, and ostracods are no longer present. Brachiopods are also diminished. Gastropods and foraminifera increase, probably due to the increased ecological space (note that bioclast abundance does not decrease compared to the 0–3 cm interval). This interval also marks the last continuous occurrence of fusulinids, and may therefore mark the beginning of the extinction, as later occurrences are sporadic and may be reworked.

From 9 to 14 cm: This is the beginning of oolite deposition. Although oolites may indicate sedimentation in an agitated environment, where wave/currents may bring oxygen to the seafloor, we propose that dysoxic-euxinic conditions remained during this interval (suggested by framboid diameters and S/C ratios). As mentioned earlier, this indicates there was a strong and consistent euxinic input capable of overcoming the oxidating environment.

From 14 to 19 cm: Although no S/C ratio or $\delta^{34}S_{sulfide}$ data is available, bioclast abundance and diversity are the same as between 9 and 14 cm, which suggests the dysoxic–euxinic conditions probably continue to 19 cm.

From 19 to 24 cm: All paleoredox indicators suggest an oxic environment (or no significant dysoxia). All fossil groups except ostracods reappear. But, as noted before, this assemblage is reduced in abundance (30% bioclast composition, compared with 50% at 14–19 cm). The reason for this is uncertain, perhaps simply due to changing physical conditions favoring oolite deposition. Fossil diversity comes at the expense of foraminfera abundance.

From 24 to 25 cm: The disappearance of fossil diversity is dramatic. All fossil groups except gastropods disappear. This sudden disappearance of biota in the Italian Dolomites is consistent with the consensus that the extinction was rapid in marine realm, possibly less than 30 000 years (Rampino and Adler, 1998; Jin et al., 2000; Twitchett et al., 2001; Erwin et al., 2002; Rampino et al., 2002). Even if we take the beginning of the extinction at 9 cm (last of the continual fusulinid occurrence) and this is the last phase of the extinction, this would represent about 5000 years (according to Rampino and Adler's, 1998, age calculation assuming sedimentation rate of 30 m/million years). This extinction level, within the first oolite bed of the Tesero Member, is consistent with other northern Italian sections (e.g., Tesero and Val Badia). Also, the presence of gastropod bioclasts following the extinction mimics the unusual micro-grastropod biofacies recognized by Fraiser et al. (2005) from the Gastropod Oolite Member of the Werfen Formation of Punta Rolle, Italy and other post-extinction successions of the world (see Fraiser et al., 2005, Table 2). This unusual gastropod biofacies was interpreted as a chemically and/or physiologically harsh environment in the recovery period (Fraiser et al., 2005).

This decline in biota coincides with a second dysoxic–euxinic interval which is more intense than the first, judging by the increased S/C ratios. We suggest that this intense dysoxic–euxinic interval dealt the final blow in the extinction process.

From 25 to 32 cm: Paleoredox conditions are similar to the earlier high S/C ratio interval (at 3–14 cm). However, the intensity or duration of euxinia is greater, suggested by the higher S/C ratios and lower $\delta^{34}S_{sulfide}$ values.

From 32 to 38 cm: There is an easing of the anoxia–euxinia, but possibly some pulses of euxinia suggested

by the lower $\delta^{34}S_{sulfide}$ values. The pyrite framboid diameter histogram for this level has too few data for a conclusive assessment of paleoredox according to this indicator. The top 1 cm of bed 8 is a non-oolitic limestone but shows no recovery of bioclast abundance or diversity.

4.3. $\delta^{34}S_{sulfate}$ at Bulla

Three $\delta^{34}S_{sulfate}$ troughs are apparent at Bulla. The latter two $\delta^{34}S_{sulfate}$ troughs coincide with high S/C ratios and very negative $\delta^{34}S_{sulfide}$ (−30‰ to −40‰), interpreted as being caused by euxinia. The coincidence of euxinia with the $\delta^{34}S_{sulfate}$ troughs at Bulla indicates that the $\delta^{34}S_{sulfate}$ decline was caused by the oxidation of ^{34}S-depleted H_2S into seawater ($\delta^{34}S$ of H_2S probably between −30‰ and −40‰, from the Bulla $\delta^{34}S_{sulfide}$ profile). However, euxinia does not coincide with the first Bulla $\delta^{34}S_{sulfate}$ trough. $\delta^{34}S_{sulfate}$ troughs independent of euxinia also occur at Balvany. This inconsistency is discussed below.

4.4. Comparison of Bulla and Balvany profiles and cause of $\delta^{34}S_{sulfate}$ swings

The Balvany section (Fig. 3), unlike Bulla, shows no correlation of high S/C ratios and lowered $\delta^{34}S_{sulfide}$. This indicates that euxinia did not coincide with the $\delta^{34}S_{sulfide}$ troughs at the Balvany site.

Two $\delta^{34}S_{sulfate}$ troughs are seen at Balvany. As at Bulla, the Balvany $\delta^{34}S_{sulfate}$ troughs coincide with troughs in $\delta^{34}S_{sulfide}$. However, as there is no evidence that these coincide with euxinia then the cause of these troughs cannot be attributed to the local oxidation of euxinic waters, as was the case at Bulla. Also in contrast to the Bulla section, the fractionation between $\delta^{34}S_{sulfate}$ and $\delta^{34}S_{sulfide}$ at Balvany remains constant (5–10‰) during the troughs (from beds 1 to 11). We conclude from this that the $\delta^{34}S_{sulfide}$ troughs were caused by the $\delta^{34}S_{sulfate}$ troughs, i.e., the fractionation remained constant while the seawater sulfate $\delta^{34}S$ varied. This is in contrast to the latter two troughs at Bulla, where oxidation of sulfide (in euxinic waters) caused the $\delta^{34}S_{sulfate}$ troughs. However, this raises the question of what caused the $\delta^{34}S_{sulfate}$ troughs at Balvany (as well as the first Bulla trough) if not oxidation of H_2S from euxinic waters.

We suggest that the mechanism of $\delta^{34}S_{sulfate}$ lowering in seawater is different but the source of ^{34}S-depleted sulfur is the same, i.e., euxinic waters. As the latter two Bulla troughs coincide with evidence of euxinia we suggest that H_2S rose from deeper waters (as per Kump et al., 2005) onto the Bulla shelf site followed by direct oxidation of the H_2S into the Bulla waters. However, the first Bulla trough and the Balvany troughs require an input of seawater already lowered in $\delta^{34}S_{sulfate}$ by the oxidation of H_2S. This could be achieved by, firstly, a degassing (as per Kaiho et al., 2006a,b) followed by oxidation of H_2S, which is then moved by seawater currents, thus transporting the lowered-$\delta^{34}S_{sulfate}$ seawater to another location. Secondly, if there was a reservoir of deeper euxinic waters it would contain both the ^{34}S-depleted H_2S and the residual ^{34}S-enriched sulfate (as noted by Kaiho et al., 2006a,b and Riccardi et al., 2006). The net $\delta^{34}S_{sulfate}$ of this mixture would be +10‰ to +12‰, the value of late Permian seawater (Claypool et al., 1980; Gorjan and Kaiho, 2007). It is feasible that an upwelling of these euxinic waters, with a rapid oxidation of H_2S along the way, could produce the Balvany (and the first Bulla) troughs if they displaced the present waters. It should also be noted that the end-Permian Meishan (China) $\delta^{34}S_{sulfate}$ profile, located on the eastern side of the ancient Tethys Sea (Fig. 4), also shows a trough near the extinction (Kaiho et al., 2001, 2006a). But this $\delta^{34}S_{sulfate}$ trough is more severe (from ~+25‰ to ~+1‰; Kaiho et al., 2001) than at Bulla and Balvany (from ~+20‰ to ~+10‰), and thus could not be explained by the 'upwelling' model. It could also indicate a more severe euxinic influence in the eastern Tethys.

A third option is presented by Riccardi et al. (2006). They have shown numerous troughs in $\delta^{34}S_{sulfate}$ (with minima less than 0‰) throughout the Changxingian of the Meishan and Shangsi sections, with the troughs at the extinction level just part of a series of $\delta^{34}S_{sulfate}$ movements. Riccardi et al. suggest that the $\delta^{34}S_{sulfate}$ troughs do not reflect the primary seawater $\delta^{34}S_{sulfate}$ movements. Rather, they result from a rise in the chemocline, bringing H_2S into the photic zone, which is then converted to elemental S (by sulfur-oxidizing bacteria) that is then deposited into the sediment at the site of oxidation or after movement by currents. The elemental S then alters the CAS as sedimentation proceeds. This model may explain the $\delta^{34}S_{sulfate}$ troughs not associated with euxinia at the Bulla and Balvany sections.

The plurality of the $\delta^{34}S_{sulfate}$ troughs, combined with the inconsistent coincidence of these troughs with euxinia and the difference in $\delta^{34}S_{sulfate}$ values, makes for a complex sulfur-cycling scenario at the end-Permian.

4.5. Cause of the end-Permian extinction

Riccardi et al.'s (2006) finding of many $\delta^{34}S_{sulfate}$ troughs throughout the Changxingian suggests that the trough at the extinction level is unrelated to the

extinction. However, the precise coincidence of the extinction with a decrease in seawater $\delta^{34}S_{sulfate}$ at the three Tethyan sites (Fig. 4) suggests a connection (Balvany, Kaiho et al., 2006b; Meishan, Kaiho et al., 2006a; Bulla, this study). Furthermore, the coincidence of euxinia with biota decline at Bulla suggests that they were causally related. Why earlier euxinic events (in the Changxingian) have little effect on the biota is a matter for further study.

The Bulla results are consistent with the conclusions of other researchers in this area (e.g., Grice et al., 2005; Kump et al., 2005), who suggest that euxinia (or anoxia) was the cause of the extinction. However, the question that arises is what caused the extinction at Balvany if euxinia was absent at the site. One possibility is that the low-$\delta^{34}S_{sulfate}$ waters, that coincide with the extinction, were lacking in oxygen, as it was used to oxidize H_2S. If this applied at Bulla (in beds 5 and 6) during the first $\delta^{34}S_{sulfate}$ trough one can see a decline in ostracod, algae, and gastropod abundance (ironically ostracods and gastropods fare best after the extinction), and a slight decline in bioclast abundance. Further work focusing on anoxia proxies in these sediments could resolve this.

5. Conclusions

Sulfur and carbon content, sulfur isotope, and pyrite framboid diameter data of the end-Permian Bulla section suggest that paleoredox conditions altered from oxic to dysoxic–euxinic environments. Paleontological analysis shows that bioclast abundance begins to decline with the onset of oolite deposition, which coincides with the first (of two) episode of dysoxia–euxinia. However, biota diversity is affected by paleoredox changes and the extinction is not complete until the more intense second dysoxic–euxinic episode. This suggests reduced oxygen conditions, and H_2S presence, were responsible for the end-Permian extinction. $\delta^{34}S_{sulfate}$ analyses from three geographically widespread end-Permian sections (Bulla, Balvany and Meishan) show an association of the $\delta^{34}S_{sulfate}$ decline with the mass extinction. The Bulla section shows evidence of euxinia coincident with $\delta^{34}S_{sulfate}$ troughs. This suggests the $\delta^{34}S_{sulfate}$ is the result of H_2S oxidation in surface waters. However, the euxinia does not coincide with the $\delta^{34}S_{sulfate}$ troughs at all sites. One possibility is that there was movement of low-$\delta^{34}S_{sulfate}$ seawater, i.e., H_2S was oxidized into surface waters and the surface waters moved to other sites; or H_2S was oxidized to elemental S, which was then transported to other sites. The Balvany section shows that the extinction does not necessarily coincide with euxinia. However, anoxia may be the cause.

Acknowledgements

The following funding for this study is acknowledged: Japan Society for the Promotion of Science (JSPS) postdoctoral fellowship to P.G., and research grant to K.K.; MEXT Grant # 17403011 to T.K.; and a Discovery Grant from the Australian Research Council (DP0452296) to Z.Q.C. The suggestions of two anonymous referees were greatly appreciated.

References

Becker, L., Poreda, R.J., Hunt, A.G., Bunch, T.E., Rampino, M., 2001. Impact event at the Permian–Triassic boundary: evidence from extraterrestrial noble gases in fullerenes. Science 291, 1530–1533.

Broglio Loriga, C., Cassinis, G., 1992. The Permo-Triassic boundary in the Southern Alps (Italy) and in adjacent Periadratic regions. In: Sweet, W.C., Yang, Z.Y., Dickins, J.M., Yin, H.F. (Eds.), Permo-Triassic Events in the Eastern Tethys. Cambridge University Press, Cambridge, pp. 78–97.

Calvert, S.E., Thode, H.G., Yeung, D., Karlin, R.E., 1996. A stable isotope study of pyrite formation in the Late Pleistocene and Holocene sediments of the Black Sea. Geochemica et Cosmochimica Acta 60, 1261–1270.

Canfield, D.E., 2001. Biogeochemistry of sulfur isotopes. In: Valley, J.W., Cole, D.R. (Eds.), Stable Isotope Geochemistry. Mineralogical Society of America, Washington, pp. 607–636.

Canfield, D.E., Raiswell, R., Westrich, J.T., Reaves, C.M., Berner, R.A., 1986. The use of chromium reduction in the analysis of reduced inorganic sulfur on sediments and shales. Chemical Geology 54, 149–155.

Cirilli, S., Pirini Radrizzani, C., Ponton, M., Radrizzani, S., 1998. Stratigraphical and palaeoenvironmental analysis of the Permian–Triassic transition in the Badia Valley (Southern Alps, Italy). Palaeogeography, Palaeoclimatology, Palaeoecology 138, 85–113.

Claypool, G.E., Holser, W.T., Kaplan, I.R., Sakai, H., Zak, I., 1980. The age curves of sulfur and oxygen isotopes in marine sulfate and their mutual interpretation. Chemical Geology 28, 199–260.

Erwin, D.H., 1994. The Permo-Triassic extinction. Nature 367, 231–236.

Erwin, D.H., Bowring, S.A., Jin, Y., 2002. End-Permian mass extinctions: a review. In: Koeberl, C., MacLeod, K.G. (Eds.), Catastrophic Events and Mass Extinctions: Impacts and Beyond. Geological Society of America, Boulder, pp. 363–383.

Fraiser, M.L., Twitchett, R.J., Bottjer, D.J., 2005. Unique microgastropod biofacies in the Early Triassic: indicator of long-term biotic stress and the pattern of biotic recovery after the end-Permian mass extinction. C. R. Paleovol 4, 475–484.

Gorjan, P., Kaiho, K., 2007. Correlation and comparison of seawater $d^{34}S_{sulfate}$ records at the Permian–Triassic transition. Chemical Geology 243, 275–285.

Golonka, J., Ford, D., 2000. Pangean (Late Carboniferous–Middle Jurassic) paleoenvironment and lithofacies. Palaeogeography, Palaeoclimatology, Palaeoecology 161, 1–34.

Grice, K., Cao, C., Love, G.D., Bottcher, M.E., Twitchett, R.J., Grosjean, E., Summons, R.E., Turgeon, S.C., Dunning, W., Jin, Y., 2005. Photic-zone euxinia during the Permian–Triassic superanoxic event. Science 307, 706–709.

Haas, J., Demeny, A., Hips, K., Vennemann, T.W., 2006. Carbon isotope excursions and microfacies changes in marine Permian–Triassic boundary sections in Hungary. Palaeogeography, Palaeoclimatology, Palaeoecology 237, 160–181.

Huey, R.B., Ward, P.D., 2005. Hypoxia, global warming, and terrestrial Late Permian extinctions. Science 308, 398–401.

Jin, Y.G., Wang, Y., Wang, W., Shang, Q.H., Cao, C.Q., Erwin, D.H., 2000. Pattern of marine mass extinction near the Permian–Triassic boundary in south China. Science 289, 432–436.

Kajiwara, Y., Yamakita, S., Ishida, K., Ishiga, H., Imai, A., 1994. Development of a largely anoxic stratified ocean and its temporary massive mixing at the Permian/Triassic boundary supported by the sulfur isotopic record. Palaeogeography, Palaeoclimatology, Palaeoecology 111, 367–379.

Kaiho, K., Kajiwara, Y., Nakano, T., Miura, Y., Kawahata, H., Tazaki, K., Ueshima, M., Chen, Z., Shi, G.R., 2001. End Permian catastrophe by a bolide impact: evidence of a gigantic release of sulfur from the mantle. Geology 29, 815–818.

Kaiho, K., Chen, Z.Q., Miura, Y., Kawahata, H., Kajiwara, Y., Sato, H., 2006a. Close-up of the end-Permian mass extinction horizon recorded in the Meishan section, South China: sedimentary, elemental, and biotic characterization with a negative shift of sulfate sulfur isotope ratio. Palaeogeography Palaeoclimatology Palaeoecology 239, 396–405.

Kaiho, K., Kajiwara, Y., Chen, Z.Q., Gorjan, P., 2006b. A sulfur isotope event at the end of the Permian. Chemical Geology 235, 33–47.

Kalliokoski, J., Cathles, L., 1969. Morphology, mode of formation, and diagenetic changes in framboids. Bulletin of the Geological Society of Finland 41, 125–133.

Kamo, S.L., Czamanske, G.K., Amelin, Y., Fedorenko, V.A., Davis, D.W., Trofimov, V.R., 2003. Rapid eruption of Siberian flood-volcanic rocks and evidence for coincidence with the Permian–Triassic boundary and mass extinction at 251 Ma. Earth and Planetary Science Letters 214, 75–91.

Kump, L.R., Pavlov, A., Arthur, M.A., 2005. Massive release of hydrogen sulfide to the surface ocean and atmosphere during intervals of oceanic anoxia. Geology 33, 397–400.

Lyons, T.W., 1997. Sulfur isotopic trends and pathways of iron sulfide formation in upper Holocene sediments of the anoxic Black Sea. Geochimica et Cosmochimica Acta 61, 3367–3382.

Massari, E., Neri, C., 1997. The infill of a supradetachment(?) basin: the continental to shallow-marine Upper Permian succession in the Dolomites and Carnia (Italy). Sedimentary Geology 110, 181–221.

Newton, R.J., Pevitt, E.L., Wignall, P.B., Bottrell, S.H., 2004. Large shifts in the isotopic composition of seawater sulphate across the Permo–Triassic boundary in northern Italy. Earth and Planetary Science Letters 218, 331–345.

Nielsen, J.K., Shen, Y., 2004. Evidence for sulfidic deep water during the late Permian in the East Greenland Basin. Geology 32, 1037–1040.

Perri, M.C., 1991. Conodont biostratigraphy of the Werfen Formation (Lower Triassic), Southern Alps, Italy. Bolletino della Societa Paleontologica Italiana 30, 23–46.

Raiswell, R., 1982. Pyrite texture, isotopic composition and the availability of iron. American Journal of Science 282, 1244–1263.

Raiswell, R., Berner, R.A., 1986. Pyrite and organic matter in Phanerozoic normal marine shales. Geochimica et Cosmochimica Acta 50, 1967–1976.

Rampino, M.R., Adler, A.C., 1998. Evidence for abrupt latest Permian mass extinction of foraminifera: results of test for the Signor–Lipps effect. Geology 26, 415–418.

Rampino, M.R., Prokoph, A., Adler, A.C., Schwindt, D.M., 2002. Abruptness of the end-Permian mass extinction as determined from biostratigraphic and cyclostratigraphic analyses of European western Tethyan sections. In: Koeberl, C., MacLeod, K.G. (Eds.), Catastrophic Events and Mass Extinctions: Impacts and Beyond. Geological Society of America, Boulder, pp. 415–427.

Retallack, G.J., 1999. Postapocalyptic greenhouse paleoclimate revealed by earliest Triassic paleosols in the Sydney Basin, Australia. Geological Society of America Bulletin 111, 52–70.

Riccardi, A.L., Arthur, M.A., Kump, L.R., 2006. Sulfur isotopic evidence for chemocline upward excursions during the end-Permian mass extinction. Geochimica et Cosmochimica Acta 70, 5740–5752.

Sweeney, R.E., Kaplan, I.R., 1980. Stable isotope composition of dissolved sulfate and hydrogen sulfide in the Black Sea. Marine Chemistry 9, 145–152.

Tucker, M.E., Wright, V.P., 1990. Carbonate Sedimentology. Blackwell Scientific Publications, Oxford. 482 pp.

Twitchett, R.J., Looy, C.V., Morante, R., Visscher, H., Wignall, P.B., 2001. Rapid and synchronous collapse of marine and terrestrial ecosystems during the end-Permian biotic crisis. Geology 29, 351–354.

Wang, Q., Morse, J.W., 1995. Laboratory simulation of pyrite formation in anoxic sediments. In: Vairavamurthy, M.A., Schoonen, M.A.A. (Eds.), Geochemical Transformations of Sedimentary Sulfur. American Chemical Society, Washington D.C., pp. 206–223.

Weidlich, O., Kiessling, W., Flugel, E., 2003. Permian–Triassic boundary interval as a model for forcing marine ecosystem collapse by long-term atmospheric oxygen drop. Geology 31, 961–964.

Wignall, P.B., Newton, R., 1998. Pyrite framboid diameter as a measure of oxygen deficiency in ancient mudrocks. American Journal of Science 298, 537–552.

Wignall, P.B., Twitchett, R.J., 2002. Extent, duration, and nature of the Permian–Triassic superanoxic event. In: Koeberl, C., McLeod, K.G. (Eds.), Catastrophic Events and Mass Extinctions: Impacts and Beyond. Geological Society of America, Boulder, pp. 395–413.

Wignall, P.B., Newton, R., 2003. Contrasting deep-water records from the Upper Permian and Lower Triassic of South Tibet and British Columbia: evidence for a diachronous mass extinction. Palaios 18, 153–167.

Wignall, P.B., Morante, R., Newton, R., 1998. The Permo-Triassic transition in Spitsbergen: $d^{13}C_{org}$ chemostratigraphy, Fe and S geochemistry, facies, fauna and trace fossils. Geological Magazine 135, 47–62.

Wilkin, R.T., Barnes, H.L., 1996. Pyrite formation by reactions of iron monosulfides with dissolved inorganic and organic sulfur species. Geochimica et Cosmochimica Acta 60, 4167–4179.

Wilkin, R.T., Barnes, H.L., Brantley, S.L., 1996. The size distribution of framboidal pyrite in modern sediments: an indicator of redox conditions. Geochimica et Cosmochimica Acta 60, 3897–3912.

Wilkin, R.T., Arthur, M.A., Dean, W.E., 1997. History of water-column anoxia in the Black Sea indicated by pyrite framboid size distributions. Earth and Planetary Science Letters 148, 517–525.

Yin, H.F., Zhang, K.X., Tong, J.N., Yang, Z.Y., Wu, S.B., 2001. The Global Stratotype Section and Point (GSSP) of the Permian–Triassic Boundary. Episodes 24, 102–114.